Exploring the potential of hydrothermal waxes derived from polyethylene: Product characterization and insights from solvent effects

Guocheng Wang[1], Haoyu Xiao[1], Małgorzata Sieradzka[2], Zuzanna Prus[2], Małgorzata Wilk[2], Aneta Magdziarz[2], Yingquan Chen[1], Haiping Yang[1], Jiawei Wang[3], Yang Yang[1*]

Affiliation

[1]*State Key Laboratory of Coal Combustion, Huazhong University of Science and Technology, Wuhan, Hubei 430074, China*

[2]*AGH University of Krakow, Mickiewicza 30 Av., 30-059 Krakow, Poland*

[3]*School of Engineering and Applied Sciences, Swansea University, Swansea SA1 8EN, UK*

[*]Corresponding author, e-mail: y.yang100@outlook.com (Y. Yang)

Abstract

The accumulation of plastic waste poses a serious environmental challenge, and traditional disposal methods have become insufficient. The autoclave hydrothermal processing method, employing supercritical water as a solvent, offers notable advantages for plastic pyrolysis, including high conversion efficiency and superior product yield. The main objective of this study is to enhance the characterisation of wax products from the hydrothermal conversion of LDPE plastic, thereby facilitating research into heavy hydrocarbons outside the gasoline and diesel range. Thus, the impact of temperature and polar solvent on the product distribution has been profoundly examined. The findings demonstrate that at temperatures below 420°C, the hydrothermal wax displays a hardness comparable to paraffin and is insoluble in conventional solvents. The solid wax product yield reached 98.8% at 425 °C, representing the optimal result among all tested conditions. The addition of polar solvents enhanced the efficiency of LDPE chain scission, whereas the presence of oxygen broadened the product distribution. Adding 100% C_2H_5OH solvent results in 78% liquid phase and 22% gas phase, while adding 100% CH_3COOH results in a reduction of carbon chains from 22.2 to 15.33. Ethanol-induced chemical cyclisation in the hydrothermal wax resulted in the formation of liquid aromatic compounds (25.96%). In contrast, acetic acid led to further cracking of the wax, leading to the production of a higher proportion of light hydrocarbons (83.2%).

Keywords: plastic recycling, hydrothermal conversion, hydrothermal wax, heavy hydrocarbons

1. Introduction

The versatile properties of plastic materials, such as durability, light weight, chemical resistance, and relatively low cost of manufacture, made them applicable in many different industrial branches, especially in engineering, packaging and automotive sectors (Andrady and Neal, 2009). Polymer materials are primarily derived from natural resources such as crude oil and natural gas. Therefore, their formation contributes to serious environmental concerns, such as depletion of non-renewable natural resources, greenhouse gas emissions, and the pollution from plastic waste (Nayanathara Thathsarani Pilapitiya and Ratnayake, 2024). In 2022, the worldwide production of plastics exceeded 400.3 million tonnes, which is 2.4% higher than the previous year and 200 times more than in the 1950s (Statistica, 2024). As both the production and the use of plastic materials over the past few decades have significantly increased, so have the environmental issues associated with plastics. Moreover, a growing number of studies highlight increasing environmental contamination by microplastics (Prus and Wilk, 2024), especially in marine habitats, as around 85% of marine litter originating from land sources is plastic (Derraik, 2002). It has been proven that microplastics can adversely affect organisms' life processes, causing a long-term risk to the ecosystem (Chang et al., 2022; Sarma et al., 2022). From another point of view, the chemical and physical properties of plastics might suggest their usefulness in terms of energy recovery.

The Higher Heating Value (HHV) of synthetic polymers ranges from 20 to 46 MJ/kg (Al-Salem and Lettieri, 2010; Barbarias et al., 2018a), which confirms their significant energy content. This makes plastics a valuable feedstock for waste-to-energy (WTE) technologies, where they can be processed to generate electricity or heat. Considering the increasing market size of plastic materials, there is a need to develop an effective plastic recycling technology, with beneficial energy recovery for economic and ecological sustainability (Wang et al., 2023).

The primary methods of plastic waste disposal are landfill and incineration. However, the inherent stability of plastics makes them challenging to degrade naturally due to the fact that during their incineration a significant number of particles and organic derivatives are generated that contribute to atmospheric pollution, such as gaseous hydrocarbons, carbon monoxide (CO), carbon dioxide (CO_2), and toxic volatile organic compounds (VOCs) (Zhang et al., 2021). Although numerous regulations have been implemented and proposed, the mechanical recycling rate for plastics remains relatively low, amounting to less than 7% in the US, which generates the most plastic waste on a global scale (Hendrickson et al., 2024; Khatun et al., 2021). Consequently, identifying a technological pathway to efficiently process substantial quantities of plastic waste has emerged as a prominent research topic (Maqsood et al., 2021).

Currently in use, conventional treatment methods, including incineration, landfill, and mechanical recycling, are insufficient and inadequate for converting plastic waste into high-value-added products, unlike thermal conversion (Al-Salem and Lettieri, 2010). Thermochemical treatment of plastics, such as hydrothermal conversion, has gained significant attention in recent years due to its ability to produce high-value products under relatively mild conditions while avoiding the formation of gaseous pollutants like dioxins (Ni et al., 2016). It enables obtaining products with a concentrated carbon number distribution by controlling the reaction conditions (e.g. temperature, reaction time, or catalyst) (Cheng et al., 2023; Fivga and Dimitriou, 2018). Products from the hydrothermal conversion of plastic encompass gaseous hydrocarbons, light oils and hydrochars (Shen, 2020). In addition, product enrichment can be enhanced by introducing specific catalysts like for example zeolite beta (Munir et al., 2020), K_2CO_3 (Martínez-Narro et al., 2024) or iron-based (Shen et al., 2022), facilitating the production of high-value-added products, including fuel oil and carbon nanotube materials (Liu et al., 2023; Yang et al., 2024). However, plastics initially yield heavy hydrocarbons ($> C_{20}$) during the chain-breaking process, which are cracked into products such as small molecule

gases and carbon deposits. In addition, at ambient temperature, heavy hydrocarbons tend to solidify into hydrothermal waxes (Artetxe et al., 2013). It has been demonstrated that elevated temperatures and pressures can facilitate efficient cleavage of the polymer chain, thereby increasing the yield of short hydrocarbon chains and the conversion rate of the process (Goto et al., 2006; Ha et al., 2024). Hydrothermal processing has garnered significant attention due to its efficiency in converting plastics into diverse products, utilizing subcritical or supercritical water as a reaction medium under heated, pressurized, and oxygen-free conditions (Dave et al., 2025). The introduction of supercritical water, defined as water at a pressure greater than 22.12 MPa and a temperature greater than 374.3 °C, has been demonstrated to enhance the cleavage of polymer bonds within synthetic materials (Zhang et al., 2022). Subcritical and supercritical conditions alter key physicochemical properties of water—such as dielectric constant, density, specific heat capacity, and viscosity—transforming it into a non-polar solvent. This facilitates the dissolution of diverse organic compounds, thereby accelerating reaction rates (Lachos-Perez et al., 2017). In contradistinction to conventional thermal degradation, supercritical conditions facilitate enhanced control over reaction pathways, thereby minimising undesirable by-products and promoting the formation of targeted hydrocarbon products (Wang et al., 2021).

In hydrothermal conversion processes, the choice of reaction medium plays a crucial role in shaping reaction pathways and product characteristics. Beyond water, which commonly serves as the base medium, additional solvents can be introduced to modify the chemical environment and enhance polymer degradation (Peng et al., 2022). Polar protic solvents such as ethanol can facilitate hydrogen transfer, cyclization, and the formation of aromatic compounds (Echaroj et al., 2023). Mild acids like acetic acid promote acid-catalyzed cleavage of polymer chains, leading to the formation of shorter hydrocarbons. Reactive oxidants such as hydrogen peroxide generate oxygen species under hydrothermal conditions, enabling oxidative degradation and broadening the product distribution (Wang et al., 2018). The use of such

solvents provides opportunities to selectively tune the composition, structure, and molecular weight of the resulting products, offering greater control over the valorization of plastic waste.

The primary components of plastic-derived, hydrothermal waxes are long-chain hydrocarbons, including paraffin and olefins, which result from the thermal decomposition and restructuring of polymers under high-temperature, high-pressure water conditions (Ding and Hesp, 2021). These compounds are commonly utilized as an industrial filler in asphalt to lower the asphalt compaction temperature and as feedstock in refineries for fuel and chemical production (Bray et al., 2020). Plastic waxes also contain small amounts of alcohols, acids, esters, and olefins and are in a solid state at room temperature. A specific type of hydrothermal wax is made from polyolefins, such as Polyethylene (PE) and Polypropylene (PP), the main components of which are olefins. With high thermal stability and low manufacturing cost, PE-waxes can be used as additives to blend with asphalt to reduce asphalt viscosity and enhance composites' high-temperature performance and ageing resistance (Abdy et al., 2022). However, these investigations remain confined to laboratory-scale experiments, with no large-scale demonstration reported to date. They can also be used as feedstock in the cracking process of refineries for the production of fuels and chemicals, which is conducive to the realization of waste utilization and the reduction of environmental pollution (Li et al., 2023). PE-waxes contain lighter hydrocarbon molecules (boiling point range of 150–200 °C), unsaturated bonds and aromatic compound components that are highly irritating to the skin, which limits the application of waxes. Although lighter hydrocarbons are removed during the distillation process, further upgraded utilization of hydrothermal waxes still needs to be explored (Patil et al., 2024).

In general, plastic-derived waxes are readily produced during hydrothermal conversion. Still, the lack of separation methods of oil and solid phases, as well as high-value application pathways, are the major concerns of this technology. The research on hydrothermal waxes

concentrates on increasing product yields and complex processes, especially for LDPE conversion. The mechanism of plastic hydrothermal conversion indicates that high-yield waxes can be produced without requiring high-temperature environments or metal-loaded catalysts (Al-Salem and Dutta, 2021). Nevertheless, current research lacks the characterisation of plastic hydrothermal waxes and exploration of solvent effects in hydrothermal conversion. Conventional analytical methods, like GC-MS, HT-GC (High-Temperature Gas Chromatography), TG and DSC (Differential Scanning Calorimetry), can only measure the relative content of each heavy hydrocarbon in hydrothermal waxes. However, they are not sufficient to quantify the individual substance products, let alone understand their structure and carbon chain length.

This study addresses a critical yet underexplored route of plastic waste valorisation by investigating the wax products obtained from the hydrothermal conversion of PE plastics—a major component of post-consumer plastics. While most previous studies have focused on thermal or catalytic conversion, this work investigates a solvent-assisted hydrothermal conversion to modulate product characteristics. By introducing a variety of selected solvents (H_2O_2, C_2H_5OH, CH_3COOH) at different concentrations and reaction temperatures, this research unveils the impact of solvent and their concentration influence the composition, molecular structure, carbon chain distribution and physicochemical properties of the wax products. This approach provides a novel route for tuning product quality during hydrothermal plastic conversion and extends current understanding of how solvent-mediated reactions can be leveraged to optimise value recovery from polyolefin waste. The findings also offer practical insights for the design of more selective and controllable upcycling processes in plastic waste management

2. Materials and Methods

2.1. Materials

Pure Polyethylene (PE) was used as the main feedstock for the hydrothermal conversion. It was selected due to its extensive usage in the manufacture of plastic packaging, such as films and shopping bags, which subsequently enter the marine environment, contributing to the accumulation of marine waste plastics. The LDPE raw material was purchased from Ruixiang Plasticizing Co. Ltd. to ensure consistent quality and purity for the experimental trials. It has a HHV of 46MJ/kg (Irgolič et al., 2024) and a bulk density of 0.89g/cm^3. The results of TGA and DSC analyses are shown in Figure S2. Chemicals: Ethanol (C_2H_5OH), Hydrogen peroxide (H_2O_2), and Acetic acid (CH_3COOH) were purchased from China National Pharmaceutical Group Chemical Reagent Co. Ltd. 0.22 μm filters were provided by General Electric Biotechnology Co. Ltd.

Raw material and produced waxes were subjected to elemental analysis using a Vario Micro cube elemental analyser (purchased from Elementar, Germany) in accordance with the Chinese national standard (GB/TGB/T 18338.2-2001).

2.2. Hydrothermal conversion

A Parr 4566 autoclave reactor with capacity of 500 mL was employed to conduct hydrothermal conversion under operating pressures up to 34.5 MPa and temperatures up to 500 °C. It is equipped with a pressure meter, safety rupture discs, inlet and outlet gas valves, valves for sampling liquid, cooling coils, and thermocouple sleeves with J-joints. The scheme of the reactor is depicted in Figure S1.

Previous studies indicate that LDPE subjected to hydrothermal processing at 425 °C for 30 minutes yields approximately 97% wax (Jin et al., 2020). However, further increases in temperature or reaction duration promote the conversion of wax into liquid oil. Therefore, the reaction time in this study was 30 min and the following temperatures were selected for the

hydrothermal conversion: 410, 420, 425, 430, 435 and 440 °C. In each experimental trial, 20 g of LDPE and 40 mL of deionised water or solvent were used. In order to investigate the impact of diverse solvents on the wax production from PE, several solutions were studied at a reaction temperature of 425°C. C_2H_5OH was employed as a polar solvent for washing and potentially dissolving certain impurities (Pan et al., 2013). H_2O_2 was utilised due to its well-documented oxidative properties, facilitating the removal of organic contaminants or enabling specific reactions during the post-treatment phase. CH_3COOH was used as a mild acid with the potential to act as a process catalyst or neutraliser, depending on the requirements of the reaction. To investigate the impact of diverse solvents on wax production, a series of experiments were conducted, wherein the following percentages of solvents were employed: 1%, 20%, and 100%.

Following the assembly of the reactor, three purges with argon were conducted to eliminate residual air within the kettle. Thereafter, the pressure was adjusted to 0.62 MPa. Heating proceeded at 8 °C/min until reaching target temperatures (410-440 °C), requiring 50-55 minutes depending on the set point, with a holding time of 30 minutes. During heating, system pressures reached 15.31, 15.86, 16.55, 16.89, 17.24, and 17.58 MPa, respectively. Maximum pressures at 425°C varied by solvent: 22.75 MPa (100% C_2H_5OH), 22.06 MPa (100% H_2O_2), and 23.44 MPa (100% CH_3COOH). Post-reaction cooling achieved 300°C within 10 minutes via water quenching, with full cooling to ambient temperature requiring 120 additional minutes. The densities of the plastic-containing mixtures with pure water, C_2H_5OH, H_2O_2, and CH_3COOH in the reactor were determined to be 0.96, 0.82, 0.97, and 1.01 g/cm^3, respectively."

Once the process was completed, the cooling water valve was opened in order to reduce the temperature of the reactor to room temperature rapidly. The pressure was recorded, and then the exhaust port was opened to allow the collection of the gas products. The kettle was transferred to a beaker and weighed. The liquid and solid hydrothermal products were separated

by filtration with filter paper, with special care taken to avoid compressing the waxy solids due to their adhesive properties. Retained wax was carefully recovered using a microspatula, with residual material removed with cotton and weighed. Residual oil retained on the filter paper was dissolved in minimal dichloromethane and allowed to evaporate to constant mass in a ventilated fume hood under dark conditions and weighed. The water and oil phases were separated by a glass separatory funnel. The oil that had formed a film on the inside of the funnel was carefully removed with cotton and weighed. This measure was included in the final oil weight.

Gas quantification was performed through a three-step analytical procedure: First, the molar quantities of initial argon and product gases were calculated from pre- and post-reaction temperature/pressure measurements using the ideal gas law (Equation S1). Second, gas chromatography data provided species-specific molar percentages, enabling calculation of total gas production via argon mass balance. This approach served to validate the termination gas quantities derived from ideal gas law calculations. Finally, the mass of each gas was calculated separately and added up to give the total gas yield (Chen et al., 2019). All the experiments were repeated three times to take the average.

$$\mathrm{Ms} = \frac{Ws}{Wr} \times 100 \qquad (1)$$

$$\mathrm{Mg} = \frac{\sum \ m \times xi \times Mi}{Wr} \times 100 \qquad (2)$$

$$\mathrm{My} = 100 - \mathrm{Ms} - \mathrm{Mg} \qquad (3)$$

Where Ms is the solid yield (wt.%); Mg is the gas yield (wt.%); My is the liquid yield (wt.%); Ws is the mass of collected solid (g); Wr is the mass of raw material (g); m is the total molar number of gas calculated by Formula S1 (mol); xi is the molar percentage of gas component provided by gas chromatography (%); Mi is the relative molecular mass of gas component (g/mol); i is the gas species index (e.g., H_2, CO, CH_4).

2.3.Analytical methods

The characteristics of hydrothermal wax were analysed using thermogravimetric analysis (TG), gas chromatography-mass spectrometry (GC-MS), Fourier transform infrared spectroscopy (FTIR), proton nuclear magnetic resonance (^{1}H NMR) and carbon nuclear magnetic resonance (^{13}C NMR). Finally, the molecular formulas were validated through the use of heteronuclear multiple bond correlation (HMBC) spectroscopy.

GC-MS

The liquid products were subjected to analysis by gas chromatography/mass spectrometry (7890B/5977A, Agilent). For the purpose of sample preparation, 50 mg of the sample was dissolved in 5 mL of dichloromethane, mixed and filtered through a 0.22 μm filter membrane. The GC-MS injector was maintained at 280 °C with a split ratio of 20:1. The samples were separated using an HP-5 MS capillary column (30 m × 0.25 mm × 0.25 μm, Agilent). The oven was set to maintain a temperature of 40 °C for 2 min, after which it was heated to 200 °C at a heating rate of 5 °C/min. Finally, the oven was heated to 280 °C at a heating rate of 10 °C/min and maintained for 2 min. The products were identified according to the National Institute of Standards and Technology Mass Spectral Library 2017 Version (NIST17.L library).

NMR

Nuclear magnetic resonance (^{1}H NMR and ^{13}C NMR) spectroscopy was performed using deuterobenzene at 600 MHz on a Bruker Avance II 600 spectrometer with relaxation times of 2 s and 5 s and 128 and 1024 scans, respectively. Heterogeneous Multiple Bond Correlation (HMBC) was employed for the detection of the wax product's structure. The analysis was performed in deuterated benzene on a Bruker Avance II 600 spectrometer at 600 MHz with a relaxation time of 2 s and 16 scans. For each sample, 100 mg of wax was dissolved in 0.6 mL of deuterated benzene and filtered through a 0.22 μm PTFE syringe filter.

FTIR

Identification of functional groups in wax samples was conducted using Fourier transform infrared spectroscopy (FTIR) manufactured by a PerkinElmer ATR-FTIR (Thermo Nicolet IS5) with a spectral range of 4000-600 cm^{-1} and 256 scans with a resolution of 4 cm^{-1}. Samples were homogenized with anhydrous potassium bromide (KBr) at a 1:100 (wax:KBr) mass ratio and compressed into translucent pellets under vacuum. Before sample analysis, background spectra were acquired using pure KBr pellets to account for environmental moisture and instrumental baselines.

TG

The thermal stability of hydrothermal waxes and oils was analysed using a thermogravimetric (TG) analyser (STA-449F3 NETZSCH). Approximately 10 mg of each sample was placed in crucible and then placed in the open oven to be heated from 20 °C to 550 °C at a rate of 10 °C/min in a nitrogen rate of 60 ml/min.

GC

The composition of the gaseous products was identified using a dual-channel gas chromatograph (Panna A91, Panna Instruments). The gas chromatography was equipped with a thermal conductivity detector (TCD) and a flame ionization detector (FID), where the following carrier gases were introduced: helium (He) and nitrogen (N_2), respectively. The TCD separated the following compounds: H_2, N_2, O_2, CO_2, CH_4 and CO on a Porapak molecular sieve column and a 5A zeolite molecular sieve column, while olefins and alkanes were separated on an Al_2O_3/KCl capillary column in FID. The column temperature was 80 ℃ and held for 4 min, then heated to 150 ℃ at a heating rate of 10 ℃/min and held for 6 min. The lower heating value (LHV) of syngas was determined based on the compositional content (in mass percentage) measured by gas chromatography according to Equation S2.

3. Results and Discussion

3.1. Influence of process temperature on wax production

The hydrothermal transformation of polyethylene (PE) was first investigated across a temperature gradient (410, 420, 430, and 440°C) using deionized water as the sole solvent to evaluate temperature effects on wax yield and product characteristics systematically. The hydrothermal experiments produced temperature-dependent phase distributions: white solid waxes were predominantly obtained at 410-430°C, while only yellow liquid oils formed at 440°C. These results are consistent with previous reports in the literature (Hou et al., 2023). After collecting and observing the wax/oil products from these initial tests, additional experiments at 425 °C and 435 °C were conducted. The product derived at 425 °C gave the most visually satisfactory results, indicating a more favourable conversion and product consistency. That is why this particular product, LDPE wax produced at 425 °C, was chosen for further analysis. Figure 1 shows the wax/oil products generated from the hydrothermal experiments at all selected temperatures.

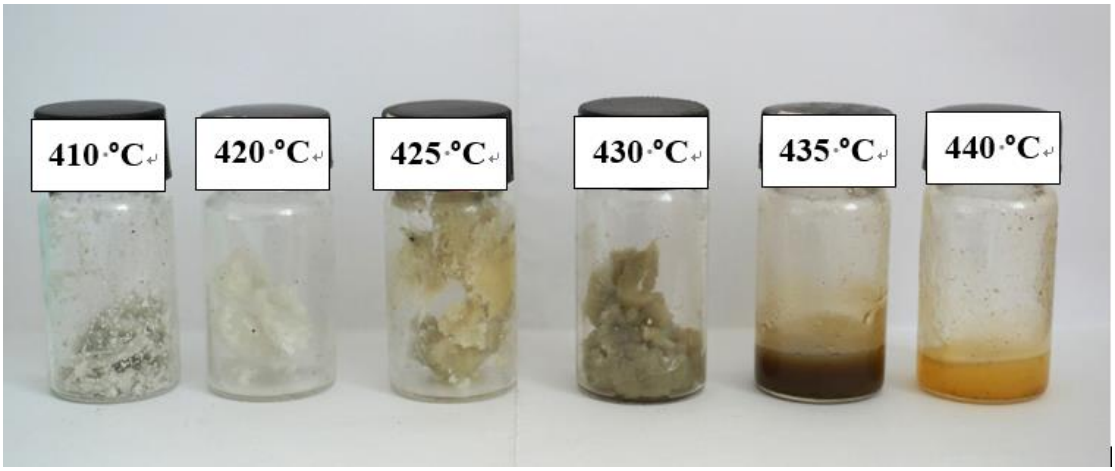

Figure 1. Wax products from the hydrothermal conversion of LDPE plastic at different temperatures.

The yields of the solid, liquid and gas products for all studied temperatures are shown in Figure 2a. Almost only solid products were obtained for the temperature of 410 °C, and no gas was detected. The solid products consist mainly of wax, and no liquid products were identified.

As the temperature increased, the liquid products were produced. For instance, at 435 °C and 440 °C, the products consisted of 96.7% and 93.9% liquid, respectively, where no wax was made. The solid yields of the products derived at 420 °C and 425 °C were similar to each other and amounted to 98.8%. Based on visual inspection of the consistency of the sample produced at 425 °C, this one was chosen as the most satisfactory. In conclusion, 425 °C was proven to be the most suitable process temperature for wax production. Figure 2b illustrates the effect of process temperature on gas production. According to the presented results, C_2 hydrocarbons were the primary gas components, with the highest yield determined for the sample derived at 440 °C, with an amount of 796.2 µmol/g, and the lowest found for the sample produced at 410 °C, with an amount of 70.2 µmol/g. It might be concluded that an increase in process temperature favours the formation of gas components, which indicates that higher process temperature provides the release of higher amounts of volatiles from raw material. The total LHV of the produced gas was measured to be 46.2-47.1 MJ/kg within the reaction temperature range of 410-440°C.

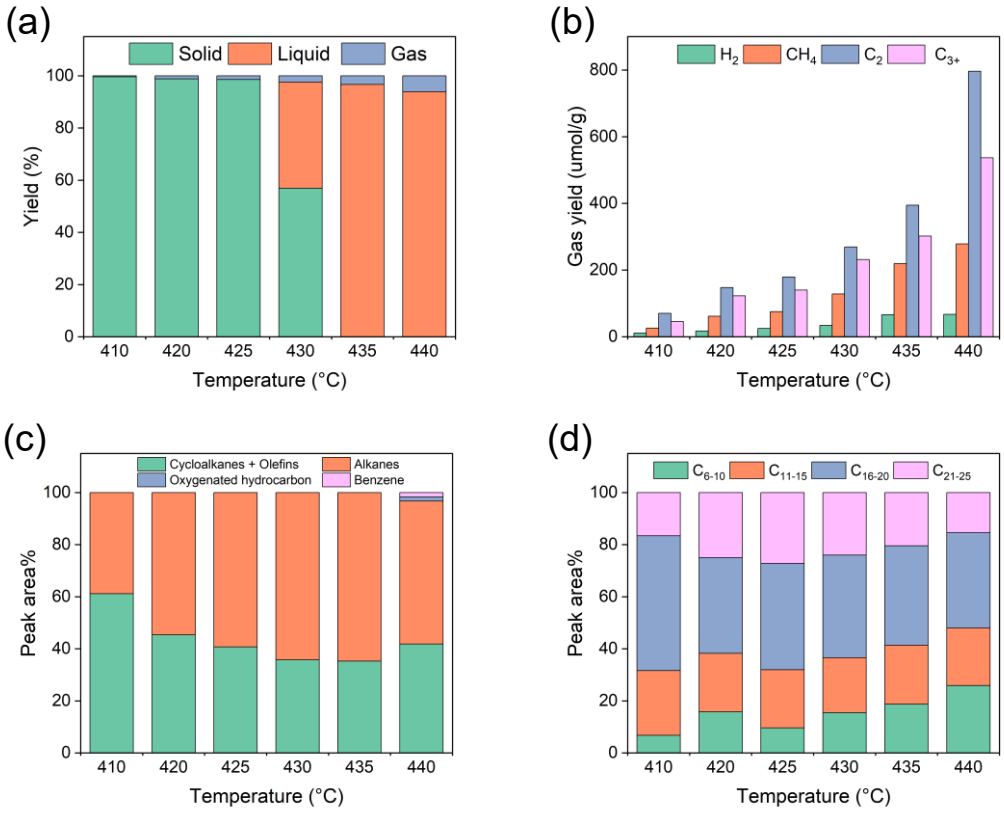

Figure 2. Characteristics of hydrothermal conversion of LDPE at different temperatures: (a) product yield; (b) gas composition; (c) distribution of products by structure; (d) distribution of products by carbon number.

The GC-MS results are presented in Figure 2c, d. It is observed that liquid samples contain hydrocarbon chains ranging from C_6 to C_{25}. It can be seen that the liquid oils are of good quality and have a distinct carbon number distribution, which can be classified into the following groups: C_6-C_{10}, C_{11}-C_{15}, C_{16}-C_{20} and C_{21}-C_{25}. Additionally, the results were categorised into the following groups: cycloalkanes plus olefins, alkanes, oxygenated hydrocarbons and benzene. It is worth noting that the solid samples produced at 410 and 420 °C could not be fully dissolved in dichloromethane. Therefore, the results at these two temperatures could not be used for comparison, and additional TG analyses were performed for the undissolved solids. As shown in Figure 2c, the waxes/oils obtained above 420 °C consisted mainly of chain alkanes, cycloalkanes and olefins, ranging from 35.3 – 41.8 wt.%. Sample of 410 °C have the highest percentage of cycloalkanes and olefins (59.2%). Small amounts of toluene and eicosanol were observed to be produced at 440 °C, with 1.6 wt.% and 1.7 wt.%, respectively. These results are consistent with previous reports (Jin et al., 2020), demonstrating that elevated temperatures or prolonged reaction times promote the conversion of cycloalkanes and olefins to aromatic compounds, albeit with limited conversion efficiency. As shown in Figure 2d, the waxes at 425 °C were mainly composed of heavy hydrocarbons with yields of 37.6 wt.% and 25 wt.% for C_{16}-C_{20} and C_{21}-C_{25}, respectively, and only 8.9 wt.% for C_6-C_{10}. As the temperature increases to 440 °C, the yield of C_{21}-C_{25} gradually decreases to 15.4 wt.% and the yield of C_6-C_{10} gradually increases to 25.9 wt.%. Results for compounds up to C_{20} can be categorised as double-bond olefins. Some compounds from C_7 to C_{17} are single-bond paraffins (Norouzi et al., 2024). This product distribution reflects the progressive chain shortening phenomenon observed across the 410-440°C temperature range. Notably, while waxes produced at 410-420°C exhibited only

partial solubility in dichloromethane, complete dissolution was achieved for the 425°C products, coinciding with the maximum concentration of C_{21}-C_{25} compounds at this optimal temperature.

The thermal cracking of waxes at different temperatures and waxes insoluble in dichloromethane at 410 and 420 °C were additionally investigated via TG (Figure 3). Decomposition of samples occurred in a one broad step, starting at 100 °C and ending at 500 °C (Figure 3a, b). The initial weight loss up to 100 °C may be related to the release of water from the sample. As shown in Figure S2, the weight loss of the initial LDPE starts at 430 °C and ends at 500 °C, with a mass loss of 56.5% at 477 °C. For most studied cases, except samples 435 °C and 440 °C, the main weight loss occurred in a temperature range of 380 – 510 °C, related to the decomposition of coke residue (Kongngoen et al., 2023). The highest weight loss rate was observed at temperature 476 °C with 58.6 % weight loss for 410 °C sample, 458 °C with 80.2% weight loss for 425 °C sample, 459 °C with 78.1% weight loss for 420 °C sample, 458 °C with 98.2% weight loss for 430 °C sample, 286 °C with 54.3% weight loss for sample 435 °C and 230 °C with 41.1% weight loss for 440 °C sample. Samples of 410 °C, 425 °C, 420 °C and 430 °C decomposed at higher temperatures due to the higher degree of crystallinity and the presence of a long-chain polymer structure in comparison to other samples (Norouzi et al., 2024). The higher processing temperature resulted in a material with a more fluid consistency, as evidenced by the photographic documentation of the samples. This phenomenon led to an increased weight loss during thermogravimetric analysis. Consequently, the thermal stability of these samples is lower than that obtained at lower temperatures.

The weight loss of insoluble waxes in dichloromethane at 410 and 420 °C occurs at 280 °C, as presented in Figures 3c and 3d. The GC-MS results (Figure 2c, d) demonstrate a distribution of products up to C_{25}, while one of the main components is alkanes. Usually, wax decomposition at temperatures lower than 225 °C is attributed to degradation of alkanes with

low molecular mass (Kongngoen et al., 2023). The undissolved wax samples obtained at 410 °C and 420 °C exhibited significant mass losses of 92.8 wt.% and 80.2 wt.%, respectively, with peak decomposition occurring at 480 °C. Consequently, the samples obtained at lower temperatures were mainly hard, heavy fractions insoluble in methylene chloride, which confirms the experimental records.

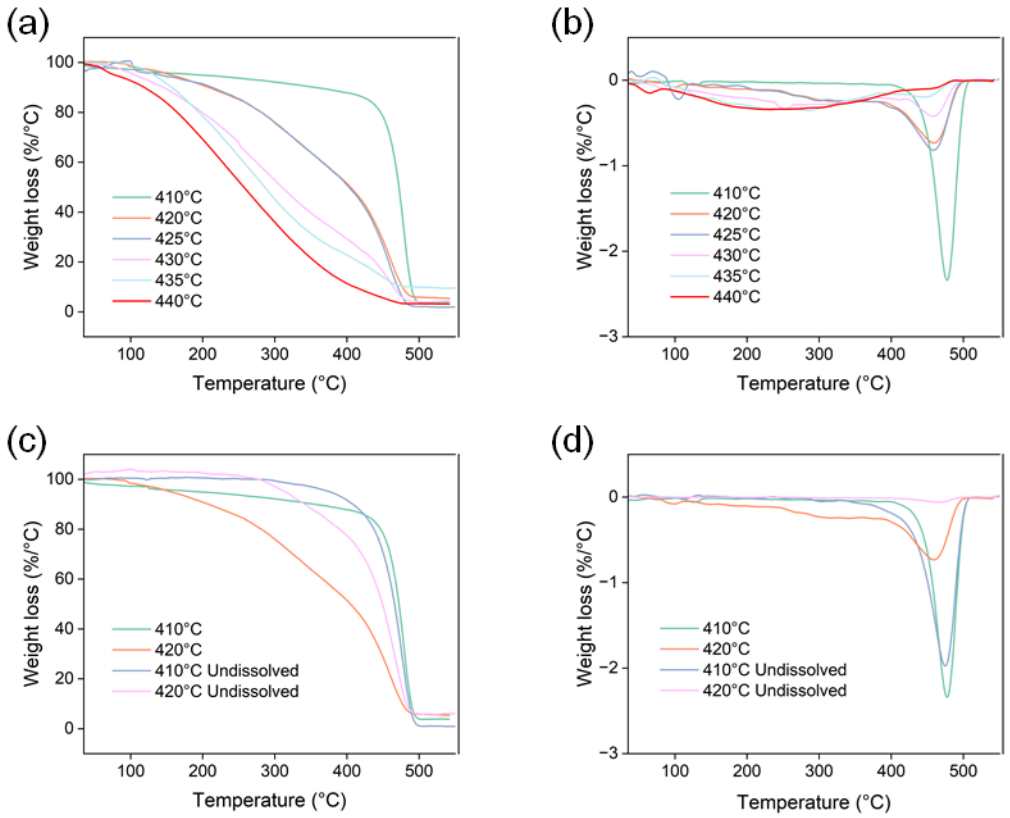

Figure 3. TG and DTG curves of wax products: (a), (b) in different temperatures; (c), (d) 410 and 420 °C wax samples insoluble in methylene chloride.

The GC-MS results do not accurately reflect the percentage of unsaturated bonds in the olefins and the carbon number distribution of the products. Therefore, waxes and oils were analysed using ^{1}H NMR to determine the changes in the distribution of unsaturated H, methylene H, and methyl H content with temperature and the structural formulae were determined by heteronuclear multiple bond correlation (HMBC). As shown by the GC-MS results, almost no benzene was produced at all temperatures, so deuterated benzene was chosen

as the solvent. The peak positions of aromatic H and aliphatic H were 6–9 ppm and 0.5–6 ppm, respectively, and the solvent peak position of deuterobenzene was 7.16 ppm (Babij et al., 2016).

The ^{1}H NMR analyses of the products at all temperatures are presented in Figure S3, which shows only the aliphatic part. The peak positions of -CH_3 substituents were in the range of 0.5–1 ppm, -CH_2-substituents were in the range of 1–1.5 ppm, -CH-substituents were in the range of 1.8–2.3 ppm, and -CH=CH- substituents were in the range of 1–2 ppm (Rudyk et al., 2023). The relative amount of each substituent was obtained by integrating the peaks over the peak area and averaging the carbon chains, employing a modification of the Cookson and Smith method (Speight et al., 2011). Carbon chain length was determined as the ratio of the intensity of the peak area of the 3-fold methylene group to that of the methyl group, plus the number of methyl groups at each end. This method can only be used for straight-chain alkanes, so the products were elementally analysed before the calculations, as shown in Table S1. The products contain minimal quantities of oxygen (O) and nitrogen (N), with the majority of their composition consisting of carbon (C) and hydrogen (H). The mole ratios of C and H for the products at LDPE and 410–440 °C are 0.47:1, 0.47:1, 0.48:1, 0.55:1, 0.47:1, and 0.54:1, respectively. The mole ratios of C and H for the products at LDPE and 410–440 °C are 0.47:1, 0.47:1, 0.48:1, 0.55:1, 0.47:1, and 0.54:1, respectively, which suggests that straight-chain alkanes are preferred to branched-chain, cycloalkane, and aromatics at the presented experimental condition.

The results of the FTIR analysis of the studied waxes are presented in Figure S4. The primary peaks identified in the FTIR analysis for each studied sample were observed at wavenumbers of 2920, 2850 and 1460 cm^{-1}. These peaks indicate long-chain aliphatic hydrocarbons, which are the main components of wax (Missau et al., 2018; Movasaghi et al., 2008). The analysis indicated that the absorption frequencies were consistent with those observed in common alkanes, thereby demonstrating similarities between the obtained samples

and paraffin waxes (Missau et al., 2018). The absorption bands at 2955, 2870, and 997 cm^{-1} correspond to -CH_3 vibrations, the absorption bands at 2917, 2852, and 910 cm^{-1} correspond to -CH_2- vibrations, and the absorption bands at 1462, 1377, and 720 cm^{-1} correspond to -CH- vibrations. These three absorption bands correspond to asymmetric stretching vibration, symmetric stretching vibration, and out-of-plane rocking vibration, respectively. In addition, the absorption bands at 1640 and 972 cm^{-1} correspond to C=C and C-C vibrations, respectively (Jung et al., 2018). As the process temperature increased, the intensity of the peaks diminished. The highest intensity was observed in the 410 °C sample, while the lowest intensity was observed in the sample obtained at 440 °C. This indicates that the quantity of identified compounds has decreased, which is consistent with the results obtained by ^{1}H NMR.

The results of the NMR parameters of hydrothermal waxes calculations are shown in Table S2. Notably, as the temperature increases from 410 to 440 °C, the methylene content decreases from 82.82% to 71.48%, while the olefinic, hypromellitic, and methyl content all increase. Therefore, the rise in temperature was favorable to increase the degree of branchedness of the product. The highest carbon chain length of 22.2 was found at 425 °C, the shortest at 440 °C was 14.83, and the carbon chain lengths of 20–22 at 410 and 420 °C were attributed to the fact that the samples obtained at these temperatures dissolved through fully deuterated benzene.

The wax products were analysed by HMBC to clarify further their structure, which provides additional information by correlating hydrogen and carbon nuclei separated by 2–3 covalent bonds. As shown in Figure 4, the upper axis is the ^{1}H spectrum and the left axis is the ^{13}C spectrum. For the ^{13}C spectrum, the peak at 127.7 ppm has the highest intensity as a solvent peak for deuterobenzene, the peaks between 10–40 ppm have the next highest intensity associated with methyl and methylene, and the peaks at 114.2 and 138.9 ppm have the lowest intensity associated with olefins (Cookson et al., 1985). The position of the peaks can be determined by their position in the carbon chain. Figure 4a, b shows that the ^{1}H peaks at 0.9

ppm and 1.36 ppm were strongly correlated with the ^{13}C peaks at 20–40 ppm and weakly correlated with the ^{13}C peaks at 114.2 and 138.9 ppm. This indicated that the dissolved wax was a straight chain with little branched chains and olefins present. However, it was observed that the ^{1}H peaks at 2.0 and 5.8 ppm were correlated with the ^{13}C peaks at 28.9 and 33.6 ppm, respectively, suggesting the presence of olefins and branched chains in the HMBC plots of waxes at other temperatures. It was noteworthy that the ^{1}H peak at 5.8 ppm showed a weak correlation with the ^{13}C peak at 33.6 ppm due to the low content of the H atom. The position of the olefin in the carbon chain was determined according to the strength of the correlation between the two olefin H. In addition, the ^{13}C peaks at 14.2 and 138.9 ppm showed a stronger correlation with the ^{1}H peak at 1.35-2.0 ppm, especially the strongest correlation with the ^{1}H peak at 2.0 ppm. This finding further validated the presence of olefins and suggested the presence of branched structures near the unsaturated carbon on the carbon chain. The waxes at 425–435 °C have similar structures. Still, an additional ^{1}H peak at 5.0 ppm can be observed in the 440 °C waxes associated with ^{13}C peaks at 114.2 and 138.9 ppm, suggesting the presence of two unsaturated carbon structures in the carbon chain. The correlation between the peaks at 0.9 ppm and 1.36 ppm in the ^{1}H spectrum and the ^{13}C peaks at 20–40 ppm was further strengthened, indicating increased branching.

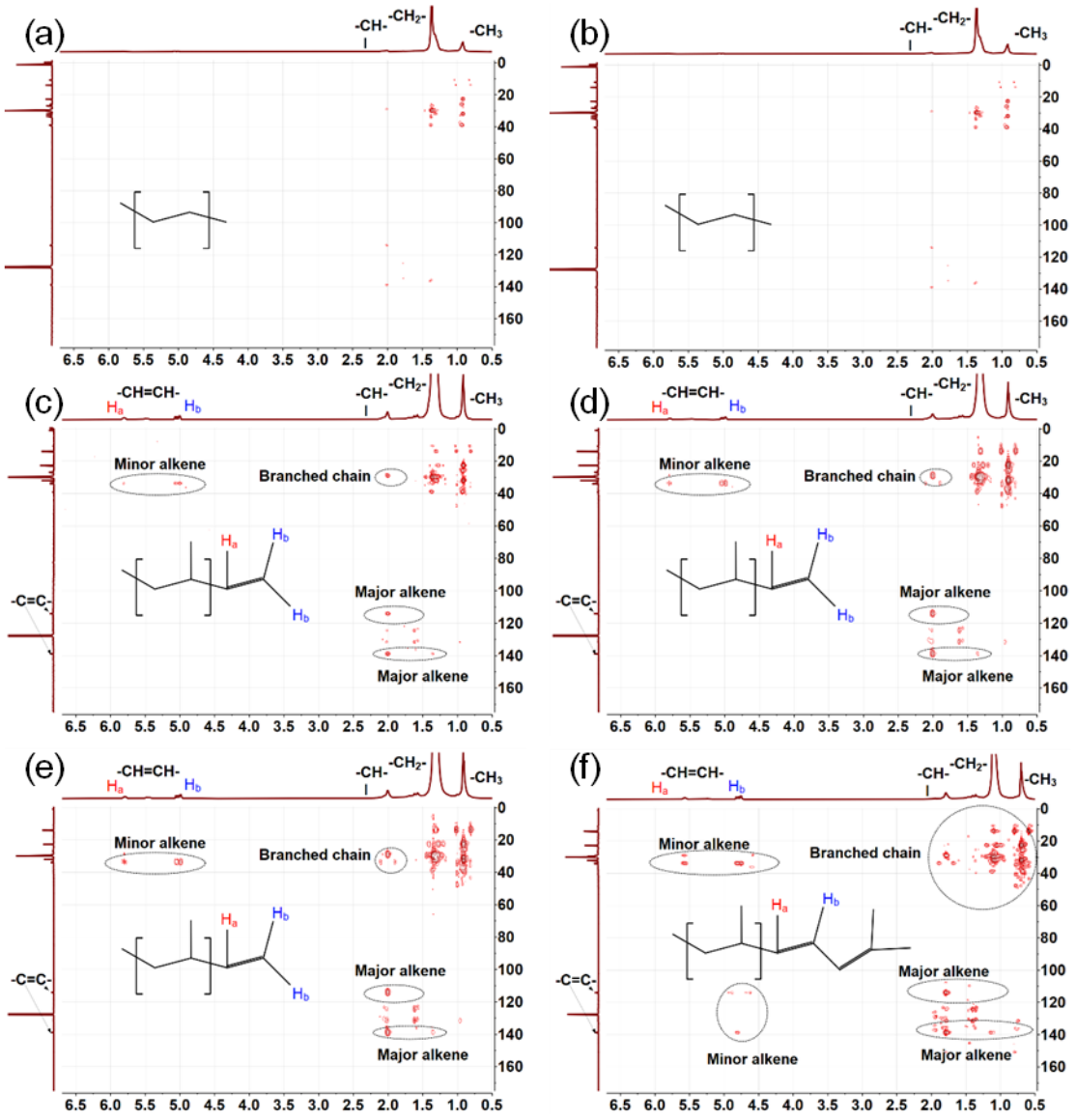

Figure 4. NMR-HMBC plots under hydrothermal wax at different temperatures: (a) 410 ℃, (b) 420 ℃,(c) 425 ℃, (d) 430 ℃, (e) 435 ℃, (f) 440 ℃.

3.2. Influence of solvents additive on the wax production at 425 ℃.

3.2.1. Hydrothermal conversion of LDPE in C_2H_5OH

The yields of the solid, liquid and gas products at different C_2H_5OH additions were shown in Figure 5a. The higher gas yield was produced as the solvent addition increased. No solid products were identified for the 100% C_2H_5OH addition, consisting of 77.8 wt.% liquid and 22.2 wt.% gas. The yield of products for 1% and 20% addition were similar, and the solid products were 98.1 wt.% and 96.2 wt.%, respectively. However, the density of the 20% addition

sample was less than the 1% addition sample based on visual inspection. This analysis suggests that adding C_2H_5OH favours the hydrothermal conversion of plastics to lower molecular weight hydrocarbons.

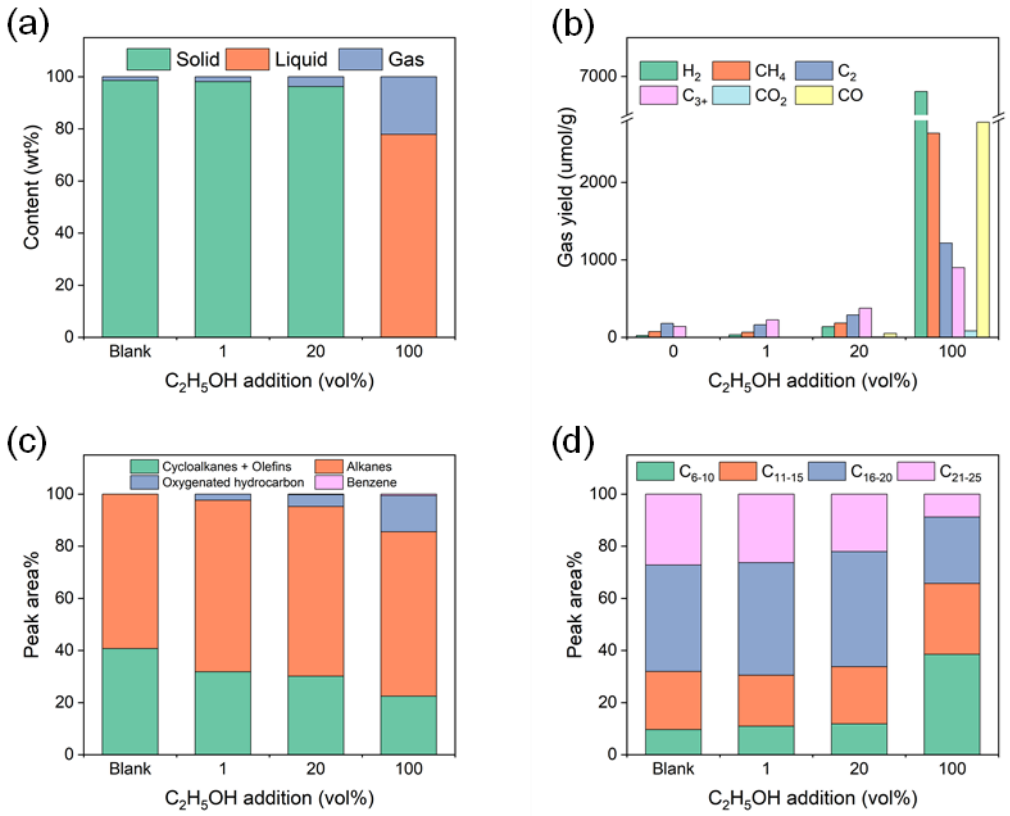

Figure 5. Hydrothermal conversion of LDPE at different concentrations of C_2H_5OH: (a) product yield; (b) gas composition; (c) distribution of products by structure; (d) distribution of products by carbon number.

Figure 5b illustrates the effect of solvent addition on gas yield. It is worth noting that alcohol tends to decompose at high temperatures to produce H_2, CH_4 and CO. The results showed that the content of C_2 and C_{3+} hydrocarbons increased with increasing C_2H_5OH content, with yields of 1216.7 μmol/g and 898.8 μmol/g for the samples at 100% C_2H_5OH addition, respectively. The total LHV of this fraction of hydrocarbons was 55.23 MJ/kg. Oxygenated compounds appear in the wax/oil after the addition of C_2H_5OH as shown in Figure 5c. With the addition of alcohol up to 100 vol%, the oxygenate content gradually increased to 13.8%,

producing a small amount of aromatic hydrocarbons. The content of chain alkanes did not change significantly, while the content of cycloalkanes and olefins gradually decreased. As shown in Fig. 5 d, at 100% C_2H_5OH addition, the oil consisted mainly of light hydrocarbons with yields of 38.5 % and 27.2 % for $C_{6\text{-}10}$ and $C_{11\text{-}15}$, respectively. However, below 20% C_2H_5OH addition, there was almost no change in the main composition of the waxes, which is consistent with the findings observed visually in the samples.

Samples with the C_2H_5OH addition had an irritant odour, especially in the case of 100% additions. As a result, the curves for TG and DTG were not stable (Figure S6). It was worth noting that the decomposition of the 100% C_2H_5OH sample, started at a temperature of 35 °C and ended at 350 °C. The results obtained for this sample differed significantly from those obtained for the others. The highest weight loss rate was observed at a temperature of 450 °C with 86.2 wt% weight loss for 1% sample, 446 °C with 91.2 wt.% weight loss for 20% sample, 167 °C with 46.3 wt.% weight loss for 100% sample. Samples of Blank, 1% and 20% C_2H_5OH additions, decomposed at higher temperatures due to the presence of a long-chain polymer structure compared to 100% of C_2H_5OH in the sample. The higher addition of C_2H_5OH resulted in a material with a more fluid consistency, which was in line with the photographic documentation depicted in Figure S4.

The results of FTIR analysis of wax under different C_2H_5OH additions were presented in Figure S7. Higher peak intensities at 1460 cm^{-1} were observed for the samples with 1% and 20% of C_2H_5OH compared to the blank sample, while the relative intensities of other characteristic peaks remained largely unchanged. This indicated that the addition of C_2H_5OH caused an increase of the number of unsaturated bonds. It was noteworthy that the curve of the sample 100% with C_2H_5OH addition exhibits additional peaks at 1120–1010 cm^{-1}, and 3100–3600 cm^{-1}, corresponding to instrumental noise, O-H stretching vibration, and C-O stretching vibration, respectively (Dutta, 2017).

According to the NMR spectra, the weaker peak intensity of $–CH_3$ and $–CH_2–$ was observed for the samples with 1% and 20% C_2H_5OH additions compared to the blank sample in Figure 6. It is noteworthy that the additional peaks appear at 3.5-4 ppm and 7.5-8 ppm in sample with 100%, corresponding to H adjacent to oxygen and H on the benzene ring, respectively. This corroborated the GC-MS results. The relative content of each peak area of the ^1H NMR spectra of the samples at different C_2H_5OH additions were shown in Table S3. The average chain length of the waxes decreased to 18.85 as C_2H_5OH addition increased to 20% and further declined to 10.97 at 100%, accompanied by a significant aromatic hydrogen proportion of 25.96%. The peak at 135 ppm in the ^{13}C NMR spectrum (Figure S8) corresponds to an aromatic structure, correlating with the peak at 7.5 ppm in ^1H NMR but not with the peak at 3.5 ppm. This suggested that the O atom was directly attached to the aromatic ring. Additionally, increasing the addition from 0% to 20% gradually enhanced each correlation signal in the HMBC spectrum, indicating that C_2H_5OH promotes branching, cyclization, and arylation in the wax.

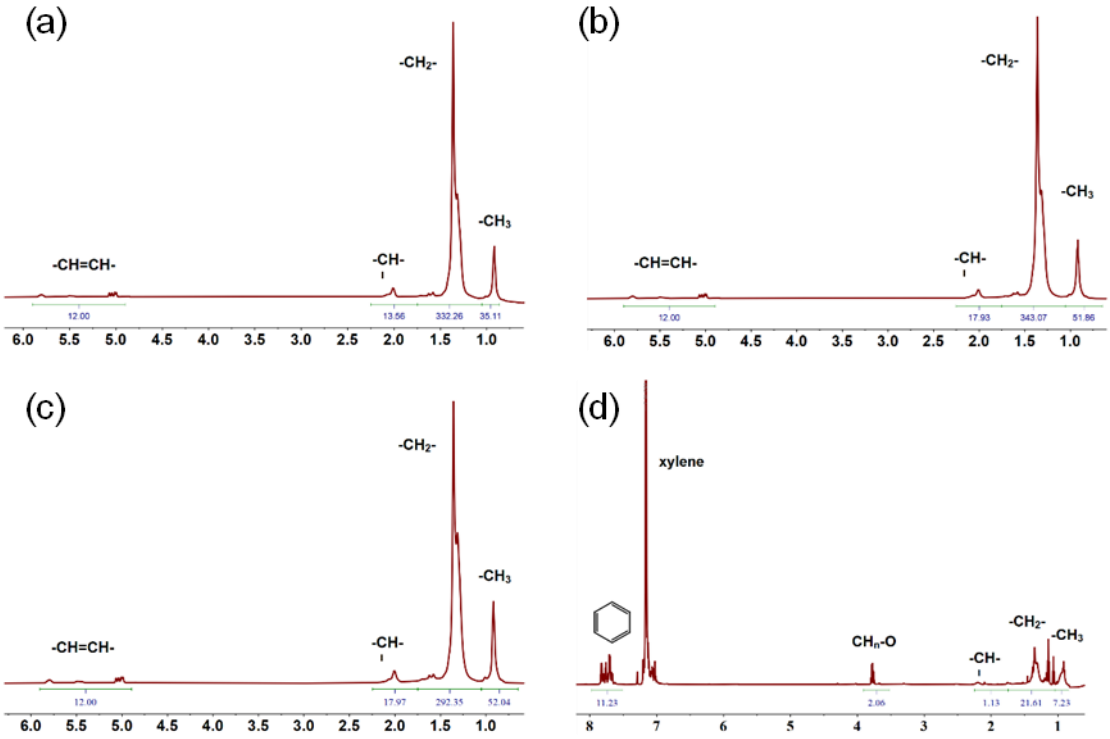

Figure 6. ^1H NMR spectra of hydrothermal waxes obtained with different concentrations of

C_2H_5OH (a) 0%, (b) 1%, (c) 20%, (d) 100%.

3.2.2. Hydrothermal conversion of LDPE in H_2O_2

The yields of the solid, liquid and gas products at different H_2O_2 additions were shown in Figure 7. All wax products were visually identified as solids. The wax yield decreased from 98.6% to 78.7 wt.% with 100% solvent addition. Although the thermal decomposition of hydrogen peroxide generated oxygen, Figure 7 b revealed significant CO and CO_2 production, indicating that the carbon source was PE. The CH_4, C_2, and C_{3+} hydrocarbons concentrations remained stable at 136.3 μmol/g, 373.5 μmol/g, and 287.7 μmol/g, respectively, regardless of the solvent addition. Conversely, H_2 yield increased with the increase of H_2O_2 addition, as the solvent became a new source of H_2 released during hydrothermal conversion. The total LHV of all combustible gases was 35.96 MJ/kg.

The addition of H_2O_2 did not significantly influence the structure of the wax products (Figure 7c) but affected the carbon number distribution (Figure 7 d). The carbon number distributions of the 20% and 100% samples were similar, with $C_{16–20}$ converting to $C_{11–15}$ compared to the blank sample, this resulted in respective contents of 26.1% and 31%. This suggested that oxygen presence led to a more disordered distribution of products below C_{20}, consistent with previous studies' findings (Xu et al., 2023).

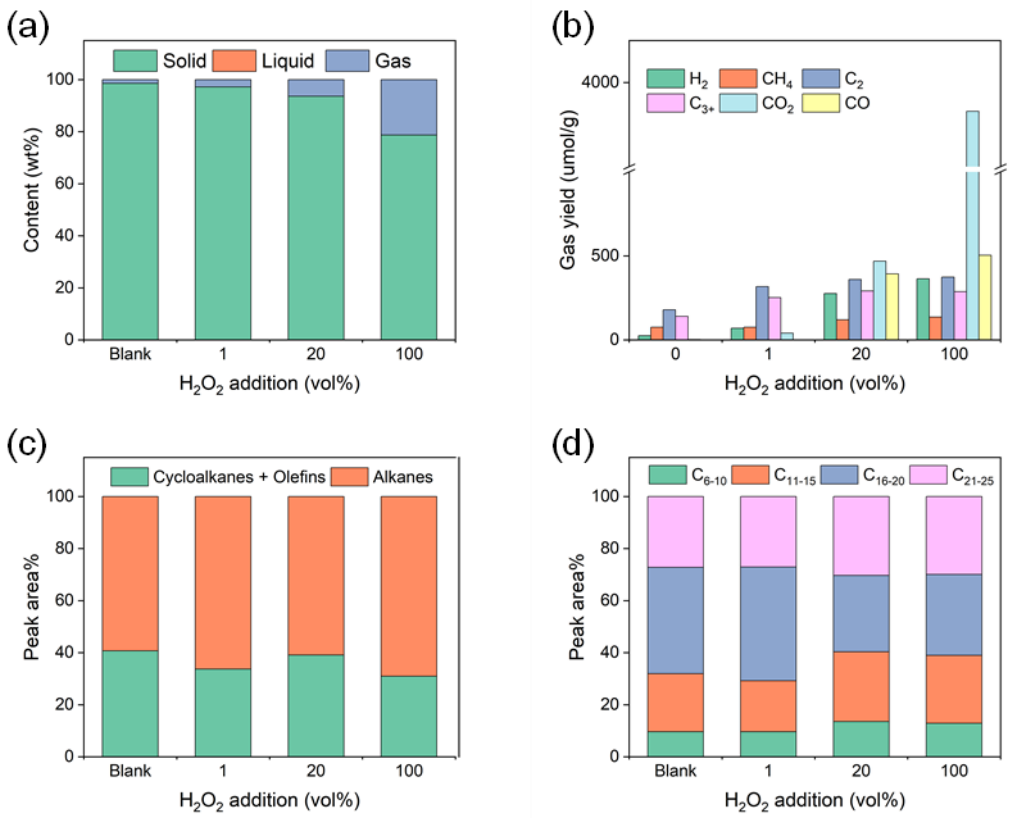

Figure 7. Characteristics of hydrothermal conversion of LDPE at different concentrations of H_2O_2: (a) product yield; (b) gas composition; (c) distribution of products by structure; (d) distribution of products by carbon number.

The TG and FTIR analyses of the 20% and 100% samples showed high similarity (Figure S10, S11). The addition of H_2O_2 did not affect the thermal behaviour of the wax, as evidenced by the comparable shapes of the curves on the graph. While the FTIR spectra exhibit prominent peaks in similar regions, with varying intensities contingent on the solvent addition. Similarly, the relative peak areas of the characteristic peaks in the ^{1}H NMR spectra (Figure S12) exhibited minimal variation. Statistical results in Table S4 indicated that the addition of hydrogen peroxide reduced the carbon chain length of the wax product from 22.2 to 19.65 while maintaining a straight-chain structure. This was attributed to the presence of oxygen, which promoted the formation of hydrocarbons within the petrol and diesel range. Additionally, visual inspection revealed that the waxes produced with hydrogen peroxide were darker (Figure S9).

3.2.3. *Hydrothermal conversion of LDPE in CH_3COOH*

The images displayed in Figure S13 illustrate the waxes obtained through the addition of varying quantities of CH_3COOH. The yields of the solid, liquid and gas products at different CH_3COOH additions were shown in Figure 8 a. Similar to the previous trend, the gas yield increased with higher solvent addition levels. Yields of 96.4 wt.% and 82 wt.% were obtained for the 1% and 20% samples, respectively. Visual inspection revealed that the 20% sample was darker in colour and less dense, while the 100% sample appeared as black liquids. This analysis suggested that the addition of CH_3COOH promoted the hydrothermal conversion of plastics into low molecular weight hydrocarbons.

Figure 8 b showed significant CH_4, CO_2, and CO production in the 100% sample, those compounds originating from the hydrothermal conversion of CH_3COOH. C_2 and C_{3+} hydrocarbons, as the primary gas components, reached their highest yields at 100% addition, measuring 640 μmol/g and 726 μmol/g, respectively, with a total LHV of 33.38 MJ/kg.

As shown in Figure 8 c, the addition of CH_3COOH did not lead to produce new compounds, but increased the content of chain hydrocarbons from 59.3% to 83.2%. Figure 8 d indicated that the 100% samples primarily consisted of light hydrocarbons, with yields of 17 wt% for $C_{6\text{-}10}$, 31.9 wt.% for $C_{11\text{-}15}$, and only 16.9 wt.% for $C_{21\text{-}25}$.

The thermal cracking of waxes at different additive levels was investigated, as shown in Figure S14. The Blank sample exhibited the highest weight loss of 80.2% at 458 °C, followed by 88% at 455 °C for the 1% sample, 92.1% at 444 °C for the 20% sample, and 44.7% at 239 °C for the 100% sample. The FTIR spectra of the samples were similar, indicating that the addition of CH_3COOH did not alter the structure of the wax products (Figure S15). As evidenced by Figure S16, the oligomer signal intensity exhibited a marked increase upon acetic acid CH_3COOH, and a small number of carbonyl peaks appeared in 20% of the samples. Statistics in Table S5 indicated that CH_3COOH reduced the carbon chain length of the wax

product from 22.2 to 15.33, for blank sample and 100% sample respectively, and increased branching. This was attributed to the chain scission of LDPE caused by the acidic environment of CH_3COOH.

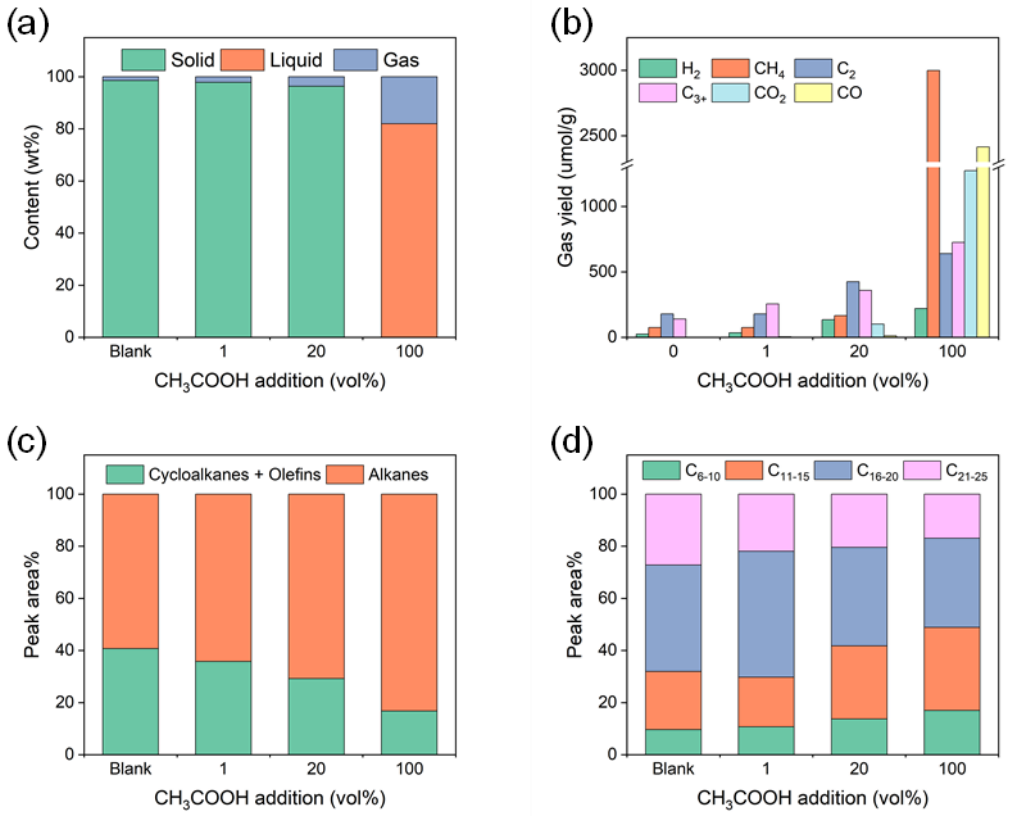

Figure 8. Hydrothermal conversion of plastics at different concentrations of CH_3COOH: (a) product yield; (b) gas composition; (c) distribution of products by structure; (d) distribution of products by carbon number.

3.3.4. Comparison of solvent effects

The influence of solvent composition and concentration on the hydrothermal depolymerization of LDPE at 425 °C revealed distinct degradation pathways, reflected in product phase distribution, carbon chain length, and molecular structure. Compared to the water-only system, which produced predominantly solid waxes with an average carbon chain length of 22.2, solvent-assisted systems exhibited enhanced chain cleavage and altered product profiles. In the presence of H_2O_2, selective chain scission was induced via oxygen-driven radical mechanisms (Zhang et al., 2023). While the overall molecular structure remained largely

583 intact, the average carbon chain length decreased to 19.65, with a higher proportion of C_{11}–C_{15}
584 hydrocarbons, indicating partial oxidative cleavage without significant branching or cyclization
585 (Cui et al., 2017). Due to its moderate acidity, CH_3COOH facilitated catalyzed β-scission and
586 hydrolytic cleavage, leading to a marked increase in low-molecular-weight hydrocarbons
587 (83.2%) and a chain length reduction to 15.33. Structural analysis showed limited aromatization
588 but substantial cracking, consistent with classical acid-catalyzed degradation (Comisar et al.,
589 2008; Yang et al., 2021). Ethanol, a polar protic solvent, promoted hydrogen transfer and
590 radical-mediated pathways, resulting in the most pronounced transformation: complete
591 liquefaction, a carbon chain length reduction to 10.97, and the highest aromatic hydrogen
592 content (25.96%), indicating extensive cyclization and aromatization (Wu et al., 2021).
593 At 100% concentrations of both ethanol and acetic acid, no solid waxes were recovered,
594 attributable to complete depolymerization and the absence of high-molecular-weight residues.
595 In contrast, solid waxes were preserved in the water-only and all H_2O_2 systems, where
596 degradation was less extensive. Intermediate concentrations (1% and 20%) of all solvents
597 revealed progressive effects: for ethanol and acetic acid, increasing concentration led to lighter,
598 less dense waxes with more pronounced chain scission and molecular rearrangement; for
599 hydrogen peroxide, chain shortening and color changes occurred gradually, with solid products
600 retained throughout.
601 Considering the findings, the addition of solvent and its concentration strongly dictates
602 both the extent and mechanism of LDPE degradation and wax formation under hydrothermal
603 conditions. Oxidizing (H_2O_2), hydrogen-donating (C_2H_5OH), and acidic (CH_3COOH) solvents
604 offer distinct pathways - oxidative cleavage, hydrogenolysis/aromatization, and acid-catalyzed
605 cracking, respectively, allowing for tunable control over product distribution (Figure 9). From
606 a product engineering perspective, ethanol is most effective for generating liquid aromatics,

acetic acid for maximizing light hydrocarbons via controlled cracking, and water-only treatment is preferred when targeting high-yield, long-chain solid waxes.

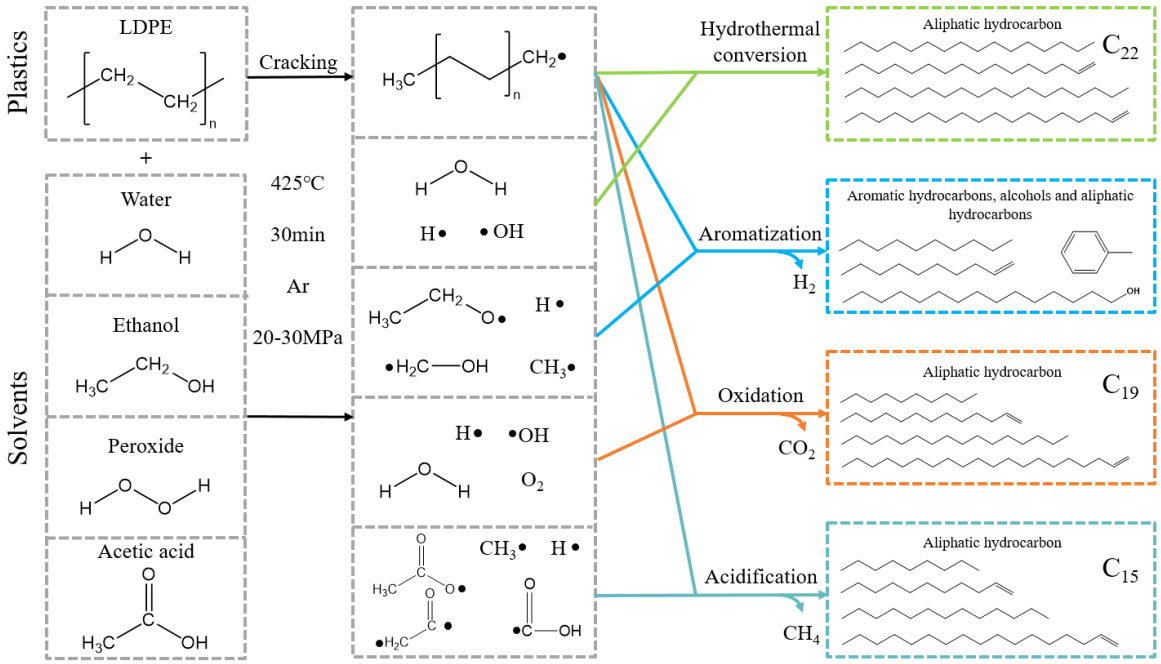

Figure 9. Main mechanisms of LDPE hydrothermal degradation in different solvents used as reaction medium

4. Conclusions

This study focuses on hydrothermal wax's characteristics using multiple analytical methods to determine its structural and chemical composition. The wax resembled hard paraffin at lower hydrothermal temperatures (410–420 °C) while it exhibited diesel-like characteristics at higher temperatures (430–440 °C). It was found that temperature significantly influenced the morphology and properties of hydrothermal wax from PE, even with a temperature variation of 5 °C. The wax obtained at 425 °C showed optimal viscosity and solubility, facilitating further processing. That is why the addition of different solvents on the wax derived at 425 °C have been extensively studied. For instance, the addition of C_2H_5OH or CH_3COOH promoted LDPE chain splitting. In particular, C_2H_5OH addition specifically enhanced the cyclization, branching,

and aromatization of the products. In the case of H_2O_2 addition, which promoted an oxygen environment, more disordered product distributions were obtained.

This work reported the hydrothermal conversion of LDPE for wax production, providing a foundation for the quantitative analysis and upgrading of hydrothermal wax and addressing the urgent challenge of plastic waste management. However, for waxes obtained at lower temperatures, the characterization methods employed in this study could not fully reveal their composition. These waxes, with morphology, structure, and hardness similar to paraffin, may serve as raw materials for phase-change materials. For softer paraffin, applications could be expanded by introducing oxygen-containing functional groups, enabling the production of soaps, surfactants, and related products. The potential of these possibilities will be investigated in greater depth in further research. In conclusion, the novel approach to plastic waste management by employing an optimal hydrothermal conversion will reduce environmental risk.

Declaration of Competing Interest

The authors declare that they have no known competing financial interests or personal relationships that could have appeared to influence the work reported in this paper.

Acknowledgments

This work was supported by the European Union HORIZON TMA MSCA Staff Exchanges program (HORIZON-MSCA-2021-SE-01) under Grant Agreement No. 101086071, as part of the project “CUPOLA – Carbon-neutral pathways of recycling marine plastic waste.” Financial support was further provided by the National Natural Science Foundation of China (Grant No. 52125601). Additional funding was provided by the Ministry of Science and Higher Education in Poland through the "PMW" program (Grant Agreement No. 5863/HE/2024/2, Project No. The authors also acknowledge the technical assistance provided by the Analytical and Testing Center of Huazhong University of Science & Technology (http://atc.hust.edu.cn).

References

Statistica, 2024. Annual production of plastics worldwide from 1950 to 2023. https://www.statista.com/statistics/282732/global-production-of-plastics-since-1950/

Abdy, C., Zhang, Y., Wang, J., Yang, Y., Artamendi, I., Allen, B., 2022. Pyrolysis of polyolefin plastic waste and potential applications in asphalt road construction: A technical review. Resources, Conservation and Recycling 180, 106213.https://doi.org/10.1016/j.resconrec.2022.106213

Al-Salem, S.M., Dutta, A., 2021. Wax Recovery from the Pyrolysis of Virgin and Waste Plastics. Industrial & Engineering Chemistry Research 60, 8301-8309.https://doi.org/10.1021/acs.iecr.1c01176

Al-Salem, S.M., Lettieri, P., 2010. Kinetic study of high density polyethylene (HDPE) pyrolysis. Chemical Engineering Research and Design 88, 1599-1606.https://doi.org/10.1016/j.cherd.2010.03.012

Andrady, A.L., Neal, M.A., 2009. Applications and societal benefits of plastics. Philosophical transactions of the Royal Society of London. Series B, Biological sciences 364, 1977-1984.https://doi.org/10.1098/rstb.2008.0304

Artetxe, M., Lopez, G., Amutio, M., Elordi, G., Bilbao, J., Olazar, M., 2013. Cracking of High Density Polyethylene Pyrolysis Waxes on HZSM-5 Catalysts of Different Acidity. Industrial & Engineering Chemistry Research 52, 10637-10645.https://doi.org/10.1021/ie4014869

Babij, N.R., McCusker, E.O., Whiteker, G.T., Canturk, B., Choy, N., Creemer, L.C., Amicis, C.V.D., Hewlett, N.M., Johnson, P.L., Knobelsdorf, J.A., Li, F., Lorsbach, B.A., Nugent, B.M., Ryan, S.J., Smith, M.R., Yang, Q., 2016. NMR Chemical Shifts of Trace Impurities: Industrially Preferred Solvents Used in Process and Green Chemistry. Organic Process Research & Development 20, 661-667.https://doi.org/10.1021/acs.oprd.5b00417

Barbarias, I., Artetxe, M., Lopez, G., Arregi, A., Bilbao, J., Olazar, M., 2018a. Influence of the conditions for reforming HDPE pyrolysis volatiles on the catalyst deactivation by coke. Fuel Processing Technology 171, 100-109.https://doi.org/https://doi.org/10.1016/j.fuproc.2017.11.003

Barbarias, I., Artetxe, M., Lopez, G., Arregi, A., Bilbao, J., Olazar, M.J.F.P.T., 2018b. Influence of the conditions for reforming HDPE pyrolysis volatiles on the catalyst deactivation by coke. 171, 100-109.https://doi.org/10.1016/j.fuproc.2017.11.003.

Bray, D.J., Anderson, R.L., Warren, P.B., Lewtas, K., 2020. Wax Formation in Linear and Branched Alkanes with Dissipative Particle Dynamics. Journal of Chemical Theory and Computation 16, 7109-7122.https://doi.org/10.1021/acs.jctc.0c00605

Chang, X., Fang, Y., Wang, Y., Wang, F., Shang, L., Zhong, R., 2022. Microplastic pollution in soils, plants, and animals: A review of distributions, effects and potential mechanisms. The Science of the total environment 850, 157857.https://doi.org/10.1016/j.scitotenv.2022.157857

Chen, W.-T., Jin, K., Linda Wang, N.-H., 2019. Use of Supercritical Water for the Liquefaction of Polypropylene into Oil. ACS Sustainable Chemistry & Engineering 7, 3749-3758.https://doi.org/10.1021/acssuschemeng.8b03841

Cheng, Y., Ekici, E., Yildiz, G., Yang, Y., Coward, B., Wang, J., 2023. Applied machine learning for prediction of waste plastic pyrolysis towards valuable fuel and chemicals production. Journal of Analytical and Applied Pyrolysis 169, 105857.https://doi.org/10.1016/j.jaap.2023.105857

Comisar, C.M., Hunter, S.E., Walton, A., Savage, P.E., 2008. Effect of pH on Ether, Ester, and Carbonate Hydrolysis in High-Temperature Water. Industrial & Engineering Chemistry Research 47, 577-584.https://doi.org/10.1021/ie0702882

Cookson, D.J., Latten, J.L., Shaw, I.M., Smith, B.E., 1985. Property-composition relationships for diesel and kerosene fuels. Fuel 64, 509-519.https://doi.org/10.1016/0016-2361(85)90086-9

Cui, Y., Zhang, M., Du, F.-S., Li, Z.-C., 2017. Facile Synthesis of H_2O_2-Cleavable Poly(ester-amide)s by Passerini Multicomponent Polymerization. ACS Macro Letters 6, 11-15.https://doi.org/10.1021/acsmacrolett.6b00833
Dave, A., Kumar, P., Reddy, S.N., 2025. Hydrothermal liquefaction: Exploring biomass/plastic synergies and pathways for enhanced biofuel production. Science of The Total Environment 969, 178909.https://doi.org /10.1016/j.scitotenv.2025.178909
Derraik, J.G.B., 2002. The pollution of the marine environment by plastic debris: a review. Marine Pollution Bulletin 44, 842-852.https://doi.org/10.1016/S0025-326X(02)00220-5
Ding, H., Hesp, S.A.M., 2021. Balancing the Use of Wax-Based Warm Mix Additives for Improved Asphalt Compaction with Long-Term Pavement Performance. ACS Sustainable Chemistry & Engineering 9, 7298-7305.https://doi.org/10.1021/acssuschemeng.1c01242
Dutta, A., 2017. Chapter 4 - Fourier Transform Infrared Spectroscopy, in: Thomas, S., Thomas, R., Zachariah, A.K., Mishra, R.K. (Eds.), Spectroscopic Methods for Nanomaterials Characterization. Elsevier, pp. 73-93.
Echaroj, S., Santikunaporn, M., Phan, A.N., 2023. Supercritical ethanol liquefaction of bamboo leaves using functionalized reduced graphene oxides for high quality bio-oil production. Renewable Energy 204, 848-857.https://doi.org/10.1016/j.renene.2022.12.110
Fivga, A., Dimitriou, I., 2018. Pyrolysis of plastic waste for production of heavy fuel substitute: A techno-economic assessment. Energy 149, 865-874.https://doi.org/10.1016/j.energy.2018.02.094
Goto, M., Sasaki, M., Hirose, T., 2006. Reactions of polymers in supercritical fluids for chemical recycling of waste plastics. Journal of Materials Science 41, 1509-1515.https://doi.org/10.1007/s10853-006-4615-2
Ha, D.T., Tong, H.D., Trinh, T.T., 2024. Insights into hydro thermal gasification process of microplastic polyethylene via reactive molecular dynamics simulations. Scientific Reports 14, 18771.https://doi.org/10.1038/s41598-024-69337-z
Hendrickson, T.P., Bose, B., Vora, N., Huntington, T., Nordahl, S.L., Helms, B.A., Scown, C.D., 2024. Paths to circularity for plastics in the United States. One Earth 7, 520-531.https://doi.org/10.1016/j.oneear.2024.02.005
Hou, J., Lian, Y., zeng, Z., Luo, H., Wang, H., Sun, Y., 2023. Converting waste agricultural film to polyethylene waxes: A mechanism and whitening study. Polymer Degradation and Stability 216, 110484.https://doi.org/10.1016/j.polymdegradstab.2023.110484
Huang, H., Wang, X., Yu, J., Chen, Y., Ji, H., Zhang, Y., Rehfeldt, F., Wang, Y., Zhang, K., 2019. Liquid-Behaviors-Assisted Fabrication of Multidimensional Birefringent Materials from Dynamic Hybrid Hydrogels. ACS Nano 13, 3867-3874.https://doi.org/10.1021/acsnano.9b00551
Irgolič, M., Čolnik, M., Kotnik, P., Čuček, L., Škerget, M., 2024. Hydrothermal recycling of polyolefins as potential alternative method for fuel production. Journal of Cleaner Production 463, 142718.https://doi.org/10.1016/j.jclepro.2024.142718
Jin, K., Vozka, P., Kilaz, G., Chen, W.-T., Wang, N.-H.L., 2020. Conversion of polyethylene waste into clean fuels and waxes via hydrothermal processing (HTP). Fuel 273, 117726.https://doi.org/10.1016/j.fuel.2020.117726
Jung, M.R., Horgen, F.D., Orski, S.V., Rodriguez C, V., Beers, K.L., Balazs, G.H., Jones, T.T., Work, T.M., Brignac, K.C., Royer, S.-J., Hyrenbach, K.D., Jensen, B.A., Lynch, J.M., 2018. Validation of ATR FT-IR to identify polymers of plastic marine debris, including those ingested by marine organisms. Marine Pollution Bulletin 127, 704-716.https://doi.org/10.1016/j.marpolbul.2017.12.061
Khatun, R., Xiang, H., Yang, Y., Wang, J., Yildiz, G., 2021. Bibliometric analysis of research trends on the thermochemical conversion of plastics during 1990–2020. Journal of Cleaner Production 317, 128373.https://doi.org/ 10.1016/j.jclepro.2021.128373

Kongngoen, P., Phetwarotai, W., Assabumrungrat, S., Phusunti, N., 2023. Possible use of spent FCC catalyst for upgrading of wax from the pyrolysis of plastics to liquid fuel. Journal of Analytical and Applied Pyrolysis 173, 106076.https://doi.org/10.1016/j.jaap.2023.106076
Lachos-Perez, D., Brown, A.B., Mudhoo, A., Martinez, J., Timko, M.T., Rostagno, M.A., Forster-Carneiro, T., 2017. Applications of subcritical and supercritical water conditions for extraction, hydrolysis, gasification, and carbonization of biomass: a critical review %J Biofuel Research Journal. 4, 611-626.https://doi.org/10.18331/brj2017.4.2.6
Li, C., Wang, H., Fu, C., Shi, S., Li, G., Liu, Q., Zhou, D., Jiang, L., Cheng, Y., 2023. Evaluation of modified bitumen properties using waste plastic pyrolysis wax as warm mix additives. Journal of Cleaner Production 405, 136910.https://doi.org/10.1016/j.jclepro.2023.136910
Liu, Q., Jiang, D., Zhou, H., Yuan, X., Wu, C., Hu, C., Luque, R., Wang, S., Chu, S., Xiao, R., Zhang, H., 2023. Pyrolysis–catalysis upcycling of waste plastic using a multilayer stainless-steel catalyst toward a circular economy. 120, e2305078120.https://doi.org/doi:10.1073/pnas.2305078120
Maqsood, T., Dai, J., Zhang, Y., Guang, M., Li, B., 2021. Pyrolysis of plastic species: A review of resources and products. Journal of Analytical and Applied Pyrolysis 159, 105295.https://doi.org/10.1016/j.jaap.2021.105295
Martínez-Narro, G., Hassan, S., Phan, A.N., 2024. Chemical recycling of plastic waste for sustainable polymer manufacturing – A critical review. Journal of Environmental Chemical Engineering 12, 112323.https://doi.org/ 10.1016/j.jece.2024.112323
Missau, J., Rocha, J.d.G.d., Dotto, G.L., Bertuol, D.A., Ceron, L.P., Tanabe, E.H., 2018. Purification of crude wax using a filter medium modified with a nanofiber coating. Chemical Engineering Research and Design 136, 734-743.https://doi.org/10.1016/j.cherd.2018.06.031
Movasaghi, Z., Rehman, S., ur Rehman, D.I.J.A.S.R., 2008. Fourier Transform Infrared (FTIR) Spectroscopy of Biological Tissues. 43, 134 - 179.https://doi.org/10.1080/05704920701829043
Munir, D., Amer, H., Aslam, R., Bououdina, M., Usman, M.R., 2020. Composite zeolite beta catalysts for catalytic hydrocracking of plastic waste to liquid fuels. Materials for Renewable and Sustainable Energy 9, 9.https://doi.org/10.1007/s40243-020-00169-3
Nayanathara Thathsarani Pilapitiya, P.G.C., Ratnayake, A.S., 2024. The world of plastic waste: A review. Cleaner Materials 11, 100220.https://doi.org/10.1016/j.clema.2024.100220
Ni, H.-G., Lu, S.-Y., Mo, T., Zeng, H., 2016. Brominated flame retardant emissions from the open burning of five plastic wastes and implications for environmental exposure in China. Environmental Pollution 214, 70-76.https://doi.org/10.1016/j.envpol.2016.03.049
Norouzi, O., Haddadi, S.A., Salaudeen, S., Soltanian, S., Bartocci, P., Arjmand, M., Dutta, A., 2024. Catalytic upgrading of polyethylene plastic waste using GMOF catalyst: Morphology, pyrolysis, and product analysis. Fuel 369, 131742.https://doi.org/10.1016/j.fuel.2024.131742
Pan, Z., Shi, Y., Liu, L., Jin, Z., 2013. Depolymerization of poly(butylene terephthalate) in sub- and supercritical ethanol in a fused silica capillary reactor or autoclave reactor. Polymer Degradation and Stability 98, 1287-1292.https://doi.org/ 10.1016/j.polymdegradstab.2013.04.004
Patil, P.B., Goswami, A.D., Pinjari, D.V., 2024. Development of industrial-grade grease from waste pyrolysis wax. Journal of the Indian Chemical Society 101, 101190.https://doi.org/10.1016/j.jics.2024.101190
Peng, Y., Wang, Y., Ke, L., Dai, L., Wu, Q., Cobb, K., Zeng, Y., Zou, R., Liu, Y., Ruan, R., 2022. A review on catalytic pyrolysis of plastic wastes to high-value products. Energy Conversion and Management 254, 115243.https://doi.org/ 10.1016/j.enconman.2022.115243
Qiao, Y., Xu, F., Xu, S., Yang, D., Wang, B., Ming, X., Hao, J., Tian, Y., 2018. Pyrolysis Characteristics and Kinetics of Typical Municipal Solid Waste Components and Their Mixture:

Analytical TG-FTIR Study. Energy & Fuels 32, 10801-10812.https://doi.org/10.1021/acs.energyfuels.8b02571
Rudyk, S., Ongarbayev, Y., Spirov, P., 2023. Feature selection in GC-MS, NMR and MALDI-TOF spectra of tar sand bitumen. Unconventional Resources 3, 61-71.https://doi.org/10.1016/j.uncres.2022.12.005
Sarma, H., Hazarika, R.P., Kumar, V., Roy, A., Pandit, S., Prasad, R.J.E.S., 2022. Microplastics in marine and aquatic habitats: sources, impact, and sustainable remediation approaches. 5, 39 - 49.https://doi.org/10.1016/j.scitotenv.2022.157857.
Shen, X., Zhao, Z., Li, H., Gao, X., Fan, X., 2022. Microwave-assisted pyrolysis of plastics with iron-based catalysts for hydrogen and carbon nanotubes production. Materials Today Chemistry 26, 101166.https://doi.org/10.1016/j.mtchem.2022.101166
Shen, Y., 2020. A review on hydrothermal carbonization of biomass and plastic wastes to energy products. Biomass and Bioenergy 134, 105479.https://doi.org/10.1016/j.biombioe.2020.105479
Speight, R.J., Rourke, J.P., Wong, A., Barrow, N.S., Ellis, P.R., Bishop, P.T., Smith, M.E., 2011. 1H and 13C solution- and solid-state NMR investigation into wax products from the Fischer–Tropsch process. Solid State Nuclear Magnetic Resonance 39, 58-64.https://doi.org/10.1016/j.ssnmr.2011.03.008
Wang, C., Wu, C., Zhang, H., Lai, J., Luo, X., Liang, Y., Tian, J., 2021. Hydrothermal treatment of petrochemical sludge in subcritical and supercritical water: Oil phase degradation and syngas production. Chemosphere 278, 130392.https://doi.org/10.1016/j.chemosphere.2021.130392
Wang, J., Ma, Y., Li, S., Yue, C., 2023. Study of HDPE plastic pyrolysis characteristics using high pressure autoclave. Journal of the Energy Institute 108, 101244.https://doi.org/10.1016/j.joei.2023.101244
Wang, M., Ma, J., Liu, H., Luo, N., Zhao, Z., Wang, F., 2018. Sustainable Productions of Organic Acids and Their Derivatives from Biomass via Selective Oxidative Cleavage of C–C Bond. ACS Catalysis 8, 2129-2165.https://doi.org/10.1021/acscatal.7b03790
Wu, X., Ma, Z., Feng, T., Zhu, C., 2021. Radical-mediated rearrangements: past, present, and future. Chemical Society Reviews 50, 11577-11613.https://doi.org/10.1039/D1CS00529D
Xu, Z., Munyaneza, N.E., Zhang, Q., Sun, M., Posada, C., Venturo, P., Rorrer, N.A., Miscall, J., Sumpter, B.G., Liu, G., 2023. Chemical upcycling of polyethylene, polypropylene, and mixtures to high-value surfactants. 381, 666-671.https://doi.org/10.1126/science.adh0993
Yang, W., Liu, R., Li, C., Song, Y., Hu, C., 2021. Hydrolysis of waste polyethylene terephthalate catalyzed by easily recyclable terephthalic acid. Waste Management 135, 267-274.https://doi.org/10.1016/j.wasman.2021.09.009
Yang, Y., Wang, G., Lei, S., Xiao, H., Yang, H., Chen, H., 2024. Coupling dechlorination and catalytic pyrolysis to produce carbon nanotubes from mixed polyvinyl chloride and polyethylene. Waste Management 178, 97-104.https://doi.org/10.1016/j.wasman.2024.02.004
Zhang, F., Li, Y., Liang, Z., Wu, T., 2022. Energy conversion and utilization in supercritical water oxidation systems: A review. Biomass and Bioenergy 156, 106322.https://doi.org/10.1016/j.biombioe.2021.106322
Zhang, F., Zhao, Y., Wang, D., Yan, M., Zhang, J., Zhang, P., Ding, T., Chen, L., Chen, C., 2021. Current technologies for plastic waste treatment: A review. Journal of Cleaner Production 282, 124523.https://doi.org/10.1016/j.jclepro.2020.124523
Zhang, Y., Wang, Q., Yalikun, N., Jiang, H., Wang, H., Wang, C., Hu, D., Hu, Y., 2023. Heterogeneous Catalytic Peroxide Oxidation Inducing Surface Reactions Toward Flotation Extraction of Hazardous Poly(Vinyl Chloride) From Waste Plastics. Industrial & Engineering Chemistry Research 62, 15136-15147.https://doi.org/10.1021/acs.iecr.3c01608